Sub-ppb Measurement of a Fundamental Band Rovibrational Transition in HD

Arthur Fast and Samuel A. Meek [*]

Max Planck Institute for Biophysical Chemistry, Am Fassberg 11, 37077 Göttingen, Germany

We report a direct measurement of the 1–0 $R(0)$ vibrational transition frequency in ground-state hydrogen deuteride (HD) using infrared-ultraviolet double resonance spectroscopy in a molecular beam. Ground-state molecules are vibrationally excited using a frequency comb referenced continuous-wave infrared laser, and the excited molecules are detected via state-selective ionization with a pulsed ultraviolet laser. We determine an absolute transition frequency of 111 448 815 477(13) kHz. The 0.12 parts-per-billion (ppb) uncertainty is limited primarily by the residual first-order Doppler shift.

Precise measurements of vibrational transition frequencies in the isotopologues of molecular hydrogen can provide a sensitive probe of fundamental physics. Because these transitions can be predicted with high precision using *ab initio* theory, comparisons between theory and experiment can be used to test quantum electrodynamics, search for new forces beyond the standard model, and determine the proton-electron and deuteron-electron mass ratios more precisely [1–4]. In recent years, many precise measurements of molecular hydrogen transition frequencies have been published [5–8], with some recent works reporting fractional uncertainties of less than one part-per-billion (ppb, 10^{-9}) on vibrational overtone and electronic transition frequencies [4,9–13]. Many of these recent experiments (with a few notable exceptions [6,9]) detect infrared absorption by hydrogen in a gas cell. In order to determine accurate transition frequencies from such measurements, the data analysis must properly account for the effect of collisions on the line shape and position [8]. If saturation techniques are used to achieve sub-Doppler resolution, the complex structure of the saturation features can complicate the determination of the line center [14].

In this work, we demonstrate a technique that avoids both of these issues by measuring the molecules in the low-density, cold environment of a supersonic molecular beam. Ground-state hydrogen deuteride (HD) molecules in the beam are vibrationally excited using a tunable continuous-wave (cw) narrow-linewidth (<100 kHz) infrared (IR) laser referenced to an optical frequency comb (OFC) for absolute accuracy. To detect the excitation efficiency, the excited molecules are state-selectively ionized using a pulsed ultraviolet (UV) laser, and the HD$^+$ ions are mass-selectively detected using a time-of-flight mass spectrometer. Based on the measured infrared spectra, we are able to determine the absolute frequency of the 1–0 $R(0)$ transition with an uncertainty of 13 kHz or 0.12 ppb fractional uncertainty.

The infrared spectroscopy laser is produced as the idler of a cw optical parametric oscillator (OPO) based on the design described by Ricciardi *et al.* [15]. The OPO uses a periodically poled lithium niobate (PPLN) crystal in a bowtie cavity to convert a ~10 W, 1064 nm pump laser into a signal beam at 1762 nm and an idler beam at 2690 nm. To measure and stabilize the idler frequency, we use a Ti: sapphire-based optically locked OFC, which has been described in detail elsewhere [16]. This comb is stabilized in such a way that the carrier-envelope offset frequency f_0 is zero and the mode number n_p has a fixed 100 MHz offset from a 1064 nm reference laser. The OPO pump beam is generated by amplifying the reference laser and thus has the same frequency, ν_p. The frequency of the signal beam ν_s is measured by frequency doubling the signal output to 881 nm using an external PPLN crystal and measuring the frequency of its beat note with the OFC, $f_{\mathrm{bn},881}$. Using this beat-note frequency, we can determine the absolute frequency of the idler beam, $\nu_i = \nu_p - \nu_s$, using

$$\nu_i = \left(n_p - \frac{n_{2s}}{2} \right) f_r + 100 \text{ MHz} - \frac{f_{\mathrm{bn},881}}{2}. \quad (1)$$

In the current measurements, the mode number of the pump beat note n_p is 281 631, and the mode number of the signal second-harmonic beat note n_{2s} is 340 364. The comb repetition rate $f_r \approx 999\,996\,455.5$ Hz is monitored during each measurement relative to a rubidium oscillator disciplined by a global navigation satellite system (GNSS)
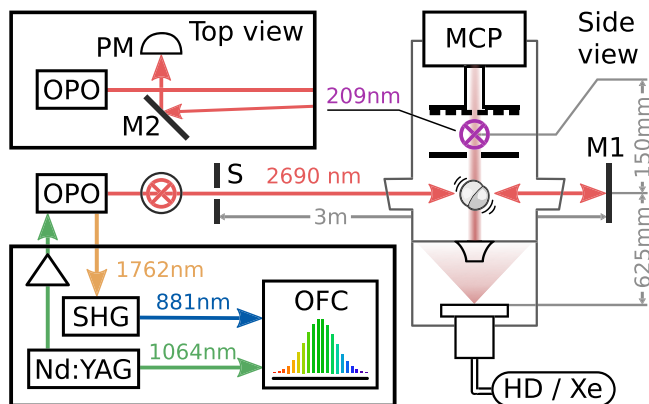
FIG. 1. Schematic overview of the experimental apparatus. The main panel shows a side view of the molecular beam. HD molecules traveling upward are first excited by a 2690 nm IR spectroscopy laser and are subsequently ionized in a time-of-flight mass spectrometer using a pulsed 209 nm UV laser. To compensate for first-order Doppler shifts, the spectroscopy laser is retroreflected from mirror $M1$ and returns through a slot S. The top left panel (Top view) shows a perpendicular view of outgoing and returning infrared beams near the OPO. The returning beam is slightly offset so that it can be separated from the outgoing beam using the mirror $M2$ and detected with a power meter (PM). The lower left panel shows the IR laser stabilization scheme.
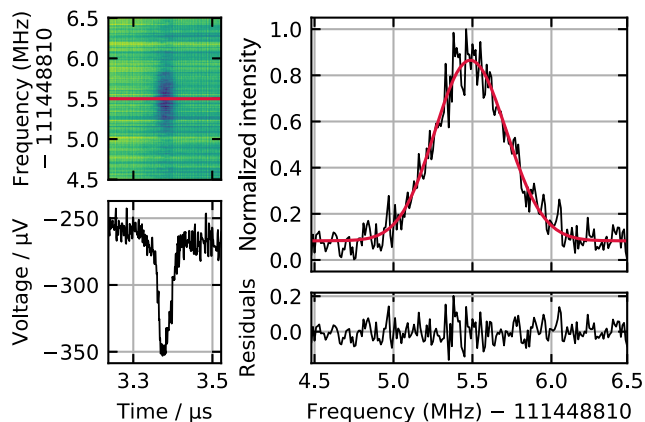

FIG. 2. Data for a typical infrared spectrum. The upper left panel shows the ion signal as a function of time delay after the ionization laser pulse and infrared laser frequency, while the lower left panel shows a cut through of this data at a single infrared laser frequency. The infrared spectrum given by the total HD^+ signal at each frequency is shown in the upper right panel in black, while the red curve shows a multi-Gaussian fit. The lower right panel shows the fit residual.

receiver. The lower left inset of Fig. 1 illustrates this scheme for measuring the idler frequency.

The main body of Fig. 1 shows the molecular beam apparatus. A 1 bar mixture of 13% HD in xenon is expanded upward through the 1 mm orifice of a room-temperature piezoactuated pulsed valve at a repetition rate of 50 Hz. Approximately 625 mm from the valve, in a second differentially pumped chamber, the molecules pass through the 1 W, 8 mm $1/e^2$ diameter infrared spectroscopy laser, and 150 mm further downstream, HD molecules in the $X^1\Sigma^+$, $v' = 1, N' = 1$ state are ionized at the entrance of a time-of-flight mass spectrometer with a pulsed UV laser using $2 + 1$ resonance-enhanced multiphoton ionization (REMPI) through the $EF^1\Sigma^+$, $v = 0, N = 1$ intermediate state. The UV laser is a frequency-tripled pulsed dye laser that produces ~ 1 mJ per pulse at 209 nm, and the pulse arrives 1.95 ms after the molecules leave the nozzle, selecting HD molecules with a velocity of 400 m/s. The extraction field in the mass spectrometer is switched on during a ± 100 μs window around the ionization pulse but is switched off while the molecules are passing through the infrared laser to minimize the static electric field in the spectroscopy region.

Spectra are measured by recording the time-resolved ion signal while scanning the frequency of the infrared laser. The upper left panel of Fig. 2 shows a typical measurement of the ion signal as a function of time delay after the laser pulse and infrared laser frequency, while the lower panel shows the ion signal versus time delay for a single laser frequency. Each time trace is averaged over approximately

1500 shots of the ionization laser, and there are 201 frequency steps in the scan. The Gaussian peak at 3.38 μs corresponds to the HD^+ mass channel. To determine the total ion intensity in this peak, the peak center and its standard deviation σ are first computed by averaging time traces at all laser frequencies and fitting the trace with the sum of a Gaussian function and a line to account for background. The ion signal is then computed at each laser frequency by averaging the signal over a $\pm 2\sigma$ region around the peak and subtracting a background calculated by averaging over regions covering $(-8\sigma, -4\sigma)$ and $(+4\sigma, +8\sigma)$ relative to the peak. The black curve in the upper right panel of Fig. 2 shows the normalized ion intensity as a function of laser frequency, while the red curve shows a fit to this data using five equal-width Gaussian peaks. The relative amplitudes and positions of these peaks (shown by the red dots in Fig. 4) are determined using a model of the hyperfine structure, and their widths are determined in the fit. Typical fitted half-maximum widths are about 400–500 kHz, which corresponds to a 3 mrad angular divergence of the molecular beam.

In order to determine the absolute 1–0 $R(0)$ transition frequency from the measured spectra, a number of potential systematic shifts have been considered. The recoil shift $h\nu_0^2/(2m_{HD}c^2) \approx 9.1$ kHz and the second-order Doppler shift $-\nu_0 v^2/(2c^2) \approx -0.1$ kHz can be computed with high accuracy and are corrected in the reported value. Other effects are found to have a negligible influence on the measured transition frequency. Based on the HD polarizability computed by Kołos et al. [17], the alternating-current (ac) Stark shift is estimated to be less than 1 Hz for the laser intensity used. External Helmholtz coils are used to reduce the magnetic field in the spectroscopy region to

below 3 μT, resulting in a residual Zeeman shift of less than 100 Hz. Assuming a density shift of -63×10^{-3} cm^{-1}/amagat (-7×10^{-17} Hz m^3) [18], xenon gas in the spectroscopy region at an estimated density of $\sim 3 \times 10^{17}$ m^{-3} would shift the transition frequency by -20 Hz. Errors in the frequency of the rubidium reference are expected to contribute less than 0.5 kHz to the overall uncertainty.

Two systematic effects are not so easily ignored and must be considered in further detail. The first and most significant is the residual shift due to the first-order Doppler effect. Although the propagation direction of the infrared laser is nominally perpendicular to the central velocity of the molecular beam, residual errors in the alignment result in a nonzero Doppler shift. To detect a misalignment, the infrared laser is retroreflected after passing through the spectroscopy region and interacts with the molecules a second time. If the retroreflection were perfect in both direction and amplitude, the Doppler shift of the second beam would be equal and opposite to the first and both beams would contribute equally to the vibrational excitation, resulting in no net shift. Unfortunately, an angular deviation between the outgoing and returning laser beams along the molecular beam direction or an imbalance of the amplitudes would result in imperfect cancellation.

To limit the angular deviation between the two beams, a 7 mm wide slot near the OPO (labeled S in Fig. 1) $\sim$3 m from the retroreflection mirror ($M1$) constrains the offset between the outgoing and returning beams along the molecular beam direction. The slot is aligned so that it is centered vertically on the outgoing beam, and the returning beam must pass through the same slot to reach a power meter (PM in Fig. 1). The returning beam is offset by about 7 mm from the outgoing beam in the direction perpendicular to the molecular beam (see the "Top view" panel of Fig. 1) to facilitate the power measurement. Based on the sensitivity of the measured power to changes of the slot height, we estimate an uncertainty of the offset between the outgoing and returning beams along the molecular beam direction of 0.5 mm, which translates to a 12 kHz uncertainty of the infrared transition frequency. This error is included both as a random error that contributes to the uncertainty of the transition frequency extracted from each spectrum and as a potential systematic error that shifts all spectra in the same direction.

The mismatch in amplitude between the two beams (caused by losses in the window and retroreflection mirror) is compensated by measuring each spectrum both with and without the retroreflected beam. If the transition frequency determined with both beams (ν_2) is the same as the frequency determined with one beam (ν_1), then the laser is perpendicular to the molecular beam, but a difference between the two frequencies indicates that ν_2 has been shifted from its true value by an amount proportional to $\nu_1 - \nu_2$. To apply this concept to the measured data, we fit all twelve measured frequency pairs (ν_1, ν_2) with a linear
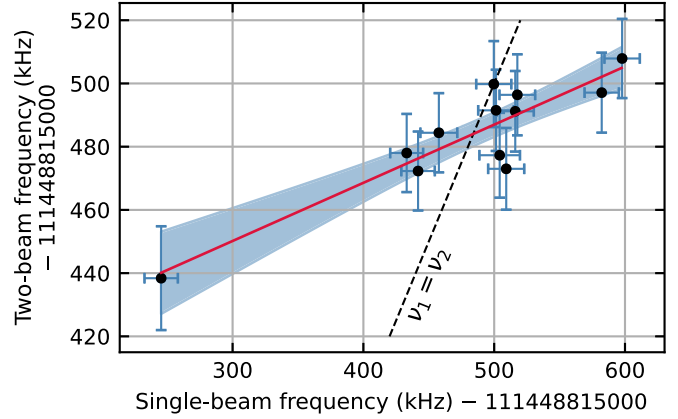

FIG. 3. Transition frequency pairs extracted from spectra measured with a retroreflected spectroscopy laser (Two-beam frequency) and with a single pass of the spectroscopy laser (Single-beam frequency) in close succession. The red line shows an orthogonal distance regression fit of the data, with a 1σ confidence region indicated in blue. The Doppler-corrected transition frequency is given by the crossing between the linear fit and the (dashed) $\nu_1 = \nu_2$ line.

model $\nu_2 = a\nu_1 + b$ using an orthogonal distance regression fit [19] in order to account for the uncertainties in both coordinates. The Doppler-corrected frequency is determined by finding the crossing point between the linear model and the line $\nu_1 = \nu_2$, which occurs at $\nu_1 = \nu_2 = b/(1-a)$. The uncertainty of this crossing point is determined by propagating the errors given by the fit covariance matrix for a and b. Figure 3 illustrates the results of such a fit.

Uncertainties in the relative intensities of the hyperfine components that make up the observed spectral profile can also contribute an error to the measured transition frequency. The $R(0)$ transition contains nine hyperfine components which, due to the degeneracy between the $F'' = 1/2$ and $F'' = 3/2$ levels in the $v'' = 0, N'' = 0$ state, results in five unique transition frequencies spread over $\sim$300 kHz. Figure 4 shows the positions of these components relative to the transition center. These individual components are not resolved in our experiment but are blended into a single $\sim$500 kHz wide peak. It is therefore important to accurately predict the relative intensities of these five components in order to correctly determine the transition center from a measured spectrum.

To model the hyperfine structure, we use an effective Hamiltonian defined by [20,21]

$$\hat{H} = T_v + B_v\hat{N}^2 - D_v\hat{N}^4 + c_{H,v}\hat{I}_H \cdot \hat{N} + c_{D,v}\hat{I}_D \cdot \hat{N}$$
$$+ \frac{eQq_{0,v}}{4I_D(2I_D - 1)}\sqrt{6}T^2_{q=0}(\hat{I}_D, \hat{I}_D) - S_v\sqrt{6}T^2_{q=0}(\hat{I}_H, \hat{I}_D).$$

$$(2)$$

A separate set of parameters is used for each vibrational state. The operator $\hat{N}$ is the rotational angular momentum,
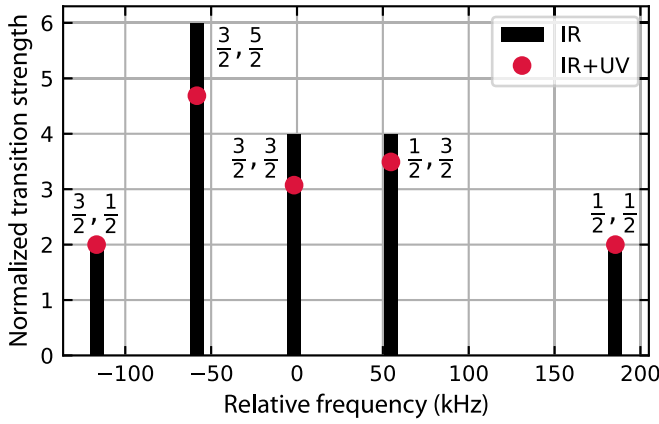
FIG. 4. Hyperfine structure of the $R(0)$ transition. The horizontal positions of the black bars show the frequencies of the hyperfine-resolved vibrational transitions relative to the line center, while their heights show the relative IR transition intensities. The fractional values next to each peak indicate the F'_1 and F' quantum numbers of the $v' = 1, N' = 1$ excited state. Red dots show the relative efficiencies for IR vibrational excitation followed by two-photon UV electronic excitation.

and $\hat{I}_H$ and $\hat{I}_D$ are the spins of the hydrogen ($I_H = 1/2$) and deuterium ($I_D = 1$) nuclei, respectively. Band origins T_v and rotational constants B_v and D_v are determined by fitting the energies calculated by the program H2Spectre [1] for the first three rotational levels in each vibrational state. The hyperfine parameters $c_{H,v}$, $c_{D,v}$, $eQq_{0,v}$, and S_v ("c_{dip}") are taken from Dupré [22]; the signs of $c_{H,v}$ and $c_{D,v}$ have been inverted to correctly reproduce the results from that work. Eigenenergies and eigenvectors based on these parameters are calculated using the program SPCAT [23]. The input files and results are included in the Supplemental Material [24].

We then define P_{IR} as the normalized sum of one-photon transition strengths from any of the degenerate $X^1\Sigma^+$, $v'' = 0, N'' = 0$ hyperfine levels to a specific M'_F level in the $X^1\Sigma^+, v' = 1, N' = 1$ state due to an IR laser polarized along the Z axis.

$$
P_{\text{IR}}(F_1{}', F', M'_F)
$$
$$
= A_{\text{IR}} \sum_{F'', M''_F} |\langle v'', N'', F_1{}'', F'', M''_F | \hat{\mu}_Z | v', N', F_1{}', F', M'_F \rangle|^2.
$$
(3)

In general, F_1 (defined by $\hat{F}_1 = \hat{N} + \hat{I}_H$) is not a good quantum number; $|v', N', F'_1, F', M'_F\rangle$ is used here as a shorthand for the eigenstate with the largest contribution from the corresponding basis vector. Because the linewidth of the UV laser is broad enough to cover all hyperfine components, the ionization efficiency from a particular M'_F level in the $X^1\Sigma^+, v' = 1, N' = 1$ state is modeled as the normalized sum of two-photon transition strengths to any

$EF^1\Sigma^+, v = 0, N = 1$ level due to a UV laser polarized along the X axis.

$$
P_{\text{UV}}(F_1{}', F', M'_F)
$$
$$
= A_{\text{UV}}
$$
$$
\times \sum_{F_1, F, M_F} |\langle X, v', N', F_1{}', F', M'_F | \hat{\mu}_X^2 | EF, v, N, F_1, F, M_F \rangle|^2.
$$
(4)

The normalization factors A_{IR} and A_{UV} are chosen such that the average values of P_{IR} and P_{UV} are 1.

The amplitudes of the black bars in Fig. 4 show the strengths of the hyperfine components of the transition calculated by summing $P_{\text{IR}}(F'_1, F', M'_F)$ over all M'_F. If the detection efficiency of the UV laser is taken into account by instead summing $P_{\text{IR}}(F'_1, F', M'_F) \times P_{\text{UV}}(F'_1, F', M'_F)$ over all M'_F, it is found that certain transitions are detected less efficiently, as indicated by the red dots. A program to compute these intensities has been included in the Supplemental Material [24]. The intensities predicted by the second model (red dots) only hold if there is no saturation of the UV transition and no reorientation of the molecules between the IR excitation and UV ionization lasers. If either of these conditions does not hold, the relative intensities of the hyperfine components will be more closely described by the first model (black bars). To account for this possibility, we analyze the measured spectra using the intensities predicted by both models and report the average of the two results as a best estimate; half of the difference is then included in the error budget. The Doppler-corrected peak position is determined to be 111 448 815.4871(47) MHz using the first model (IR only) and 111 448 815.4840(47) MHz using the second (IR and UV), resulting in an average of 111 448 815.4856(47) MHz.

Table I summarizes the contributions to the measured transition frequency. After correcting for shifts due to recoil and second-order Doppler effects, we conclude an absolute frequency for the HD 1–0 $R(0)$ transition of 111 448 815 .477(13) MHz, with the uncertainty dominated by residual first-order Doppler shifts. Table II shows a comparison

TABLE I. Frequency and uncertainty contributions to the determination of the 1–0 $R(0)$ transition frequency.

Contribution	Frequency [kHz]	σ [kHz]
Doppler-corrected peak position	111 448 815 485.6	4.7
First-order Doppler	0	12
Hyperfine	0	1.6
Frequency reference error	0	<0.5
ac Stark, Zeeman, Pressure	0	<0.1
Recoil	−9.1	0
Second-order Doppler	+0.1	0
Total	111 448 815 477	13

TABLE II. Comparison between the HD 1–0 $R(0)$ transition frequency determined in the present work and previous experimental and theoretical values.

	Frequency [MHz]	Deviation [MHz]
This work	111 448 815.477(13)	
[25] (experimental)	111 448 806(30)	10(30)
[6,26] (experimental)	111 448 818.5(6.6)	−3.0(6.6)
[1] (theoretical)	111 448 814.5(6)	1.0(6)

between this result and previous theoretical and experimental values. The theoretical value is computed using H2Spectre [1]. The present result agrees with all previous values but shows a much smaller uncertainty. Interestingly, we note that six other measurements of hydrogen vibrational transition frequencies [5,7,8,12–14], covering all three stable isotopologues, show fractional deviations from the theoretical predictions from H2Spectre consistent with the 8.7×10^{-9} deviation measured here to within experimental uncertainty.

The precision of the current result is limited primarily by residual first-order Doppler shifts and possible shifts due to unresolved hyperfine structure. We anticipate that, by improving the retroreflection quality and characterizing the hyperfine effects by changing the relative polarizations between the two lasers, the uncertainty can be reduced below 1 kHz, or 10^{-11} fractional uncertainty. Measurements at this level of precision, combined with accurate theoretical predictions, would result in values for the proton-electron and deuteron-electron mass ratios that are more precise than the 2018 CODATA recommended values [27]. With improved sensitivity, the same techniques used here could also be used to measure quadrupole transitions in the homonuclear isotopologues, making it possible to investigate the properties of the proton and deuteron separately.

---

[*]samuel.meek@mpibpc.mpg.de

[1] J. Komasa, M. Puchalski, P. Czachorowski, G. Łach, and K. Pachucki, Phys. Rev. A **100**, 032519 (2019).

[2] E. J. Salumbides, W. Ubachs, and V. I. Korobov, J. Mol. Spectrosc. **300**, 65 (2014).

[3] E. J. Salumbides, A. N. Schellekens, B. Gato-Rivera, and W. Ubachs, New J. Phys. **17**, 033015 (2015).

[4] L.-G. Tao, A.-W. Liu, K. Pachucki, J. Komasa, Y. R. Sun, J. Wang, and S.-M. Hu, Phys. Rev. Lett. **120**, 153001 (2018).

[5] C.-F. Cheng, Y. R. Sun, H. Pan, J. Wang, A.-W. Liu, A. Campargue, and S.-M. Hu, Phys. Rev. A **85**, 024501 (2012).

[6] M. L. Niu, E. J. Salumbides, G. D. Dickenson, K. S. E. Eikema, and W. Ubachs, J. Mol. Spectrosc. **300**, 44 (2014).

[7] D. Mondelain, S. Kassi, T. Sala, D. Romanini, D. Gatti, and A. Campargue, J. Mol. Spectrosc. **326**, 5 (2016).

[8] P. Wcisło, F. Thibault, M. Zaborowski, S. Wójtewicz, A. Cygan, G. Kowzan, P. Masłowski, J. Komasa, M. Puchalski, K. Pachucki, R. Ciuryło, and D. Lisak, J. Quant. Spectrosc. Radiat. Transfer **213**, 41 (2018).

[9] R. K. Altmann, L. S. Dreissen, E. J. Salumbides, W. Ubachs, and K. S. E. Eikema, Phys. Rev. Lett. **120**, 043204 (2018).

[10] F. M. J. Cozijn, P. Dupré, E. J. Salumbides, K. S. E. Eikema, and W. Ubachs, Phys. Rev. Lett. **120**, 153002 (2018).

[11] E. Fasci, A. Castrillo, H. Dinesan, S. Gravina, L. Moretti, and L. Gianfrani, Phys. Rev. A **98**, 022516 (2018).

[12] M. Zaborowski, M. Słowiński, K. Stankiewicz, F. Thibault, A. Cygan, H. Jóźwiak, G. Kowzan, P. Masłowski, A. Nishiyama, N. Stolarczyk, S. Wójtewicz, R. Ciuryło, D. Lisak, and P. Wcisło, Opt. Lett. **45**, 1603 (2020).

[13] M. L. Diouf, F. M. J. Cozijn, K.-F. Lai, E. J. Salumbides, and W. Ubachs, Phys. Rev. Research **2**, 023209 (2020).

[14] M. L. Diouf, F. M. J. Cozijn, B. Darquié, E. J. Salumbides, and W. Ubachs, Opt. Lett. **44**, 4733 (2019).

[15] I. Ricciardi, E. De Tommasi, P. Maddaloni, S. Mosca, A. Rocco, J.-J. Zondy, M. De Rosa, and P. De Natale, Mol. Phys. **110**, 2103 (2012).

[16] A. Fast, J. E. Furneaux, and S. A. Meek, Phys. Rev. A **98**, 052511 (2018).

[17] W. Kołos and L. Wolniewicz, J. Chem. Phys. **46**, 1426 (1967).

[18] S. Nazemi, A. Javan, and A. S. Pine, J. Chem. Phys. **78**, 4797 (1983).

[19] P. T. Boggs and J. E. Rogers, Report No. NISTIR 89-4197, Technical Report, NBS, Gaithersburg, MD, 1989.

[20] J. M. Brown and A. Carrington, in *Rotational Spectroscopy of Diatomic Molecules* (Cambridge University Press, Cambridge, England, 2003), pp. 342, 561.

[21] R. E. Davis and J. S. Muenter, J. Chem. Phys. **57**, 2836 (1972).

[22] P. Dupré, Phys. Rev. A **101**, 022504 (2020).

[23] H. M. Pickett, J. Mol. Spectrosc. **148**, 371 (1991).

[24] See Supplemental Material at http://link.aps.org/supplemental/10.1103/PhysRevLett.125.023001 for SPCAT input and output files and a program that evaluates Eqs. (3) and (4).

[25] N. H. Rich, J. W. C. Johns, and A. R. W. McKellar, J. Mol. Spectrosc. **95**, 432 (1982).

[26] B. J. Drouin, S. Yu, J. C. Pearson, and H. Gupta, J. Mol. Struct. **1006**, 2 (2011).

[27] E. Tiesinga, P. J. Mohr, D. B. Newell, and B. N. Taylor, The 2018 CODATA Recommended Values of the Fundamental Physical Constants (Web Version 8.1), 2020.